

From multiferroics to cosmology: Scaling behaviour and beyond in the hexagonal manganites

S. M. Griffin,¹ M. Lilienblum,¹ K. Delaney,² Y. Kumagai,¹ M. Fiebig,¹ and N. A. Spaldin¹

¹*Department of Materials, ETH Zurich, Wolfgang-Pauli-Strasse 10, CH-8093 Zurich, Switzerland*

²*Materials Research Laboratory, University of California, Santa Barbara, California 93106, USA*

(Dated: September 23, 2018)

We show that the improper ferroelectric phase transition in the multiferroic hexagonal manganites displays the same symmetry-breaking characteristics as those proposed in early-universe theories. We present an analysis of the Kibble-Zurek theory of topological defect formation applied to the hexagonal manganites, discuss the conditions determining the range of cooling rates in which Kibble-Zurek behavior is expected, and show that recent literature data¹ are consistent with our predictions. We explore experimentally for the first time to our knowledge the cross-over out of the Kibble-Zurek regime² and find a surprising “anti-Kibble-Zurek” behavior.

A key open question in cosmology is whether the vacuum contains topological defects such as cosmic strings³⁻⁷. The formation of topological defects during phase transitions in the early universe – believed in grand unified theories to occur within around 10^{-34} s after the Big Bang – was proposed by Kibble⁸, who derived the symmetry requirements for formation of topological defects in a physical manifold. In systems where such defects are symmetry allowed, their density can be estimated using the Zurek scenario⁹, which uses causality arguments to develop scaling laws for the density of defects formed as a function of the rate of quenching across the phase transition. The resulting combination of symmetry requirements and scaling laws is termed the Kibble-Zurek mechanism, and in principle should describe a phase transition in any system with the required symmetry properties, provided that other effects do not dominate the kinetics of topological defect formation.

Attempts to demonstrate Kibble-Zurek scaling in condensed-matter systems to date have proved challenging, however, and the “ideal Kibble-Zurek system” has remained elusive. Zurek’s original paper⁹ discussed the analogue between cosmic strings and the vortex cores formed in a quench-induced phase transition from normal-state to superfluid ⁴He. However the corresponding experiment^{10,11} yielded large deviations from the predicted behavior, probably because of thermal effects¹². In ³He the symmetry breaking is closer to that postulated for the early universe^{13,14}, but the density of topological defects can only be inferred indirectly and many assumptions must be made to compare with predictions. In superconducting Nb rings the density of vortex cores in the superconducting current led to a different scaling exponent than that predicted by the Kibble-Zurek mechanism – again, experimental artifacts were held responsible¹⁵ – and no flux-line formation at all was observed in experiments on high- T_C superconducting thin films¹⁶. Bose-Einstein condensates could in principle provide a suitable system but are so far subject to experimental limitations¹⁷. Perhaps the best candidates to date have been liquid crystals, in which the diffraction pattern formation in nonlinear-optic experiments has been shown

to exhibit power-law scaling¹⁸ and promising studies of defect dynamics have been performed¹⁹, but strong interactions between the defects continue to cause difficulties.

Here we propose the multiferroic hexagonal manganites, $RMnO_3$, $R = \text{Sc, Y, Dy} - \text{Lu}$, as a model system for testing the Kibble-Zurek mechanism. The hexagonal manganites have attracted interest because of their unusual geometrically-driven improper ferroelectricity, which allows for the simultaneous occurrence of magnetic ordering^{20,21}, as well as unusual couplings²²⁻²⁴ and functionalities²⁵ at their domain walls. In this work we show that the unusual nature of the improper geometric ferroelectric phase transition also sets both the correct symmetry conditions for Kibble-Zurek behavior to manifest, as well as the physical properties for readily detecting it. In addition, the relevant time-, temperature- and length-scales fall into a range that allows exploration of the Kibble-Zurek regime, as well as the crossover out of it.

I. SYMMETRY AND PHYSICAL PROPERTIES OF $RMnO_3$

First we describe the properties of $RMnO_3$ that are relevant for testing the Kibble-Zurek mechanism, particularly the symmetry properties of the phase transition. The structure of $RMnO_3$ consists of planes of MnO_5 trigonal bipyramids separated by planes of R ions which form a hexagonal mesh (Fig. 1(a))²⁶. In the high-temperature paraelectric phase, the space group is centrosymmetric $P6_3/mmc$. At $T_C \sim 1400$ K (the exact value depends on the R ion) a spontaneous symmetry breaking occurs, with the condensation of primarily two phonon modes with distinct irreducible representations of the high-symmetry structure^{21,27}. First, a mode of K_3 symmetry, which involves a trimerizing tilt of the trigonal bipyramids and is the primary order parameter (Fig. 1(b)). Since the K_3 mode can condense about three different origins, and the tilt can be in the “in” or “out” direction, six trimerization domains are formed; these have been shown using high resolution transmission elec-

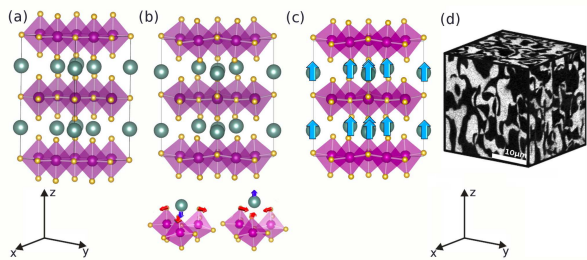


FIG. 1: (a) High-symmetry $P6_3/mmc$ structure of $RMnO_3$ before the onset of trimerization. (b) Action of the K_3 trimerization mode on the R ions and MnO_5 trigonal bipyramids. The insets below the main structure are to emphasize that outward trimerization results in a downward shift of the corresponding R ion, whereas inward trimerization results in an upward shift. (c) The subsequent additional displacements of the R ions (blue arrows) in the Γ_2^- mode provide the ferroelectricity. Note that once the orientation of the trimerization mode is set, the spontaneous polarization can emerge in only one direction. (d) Typical domain structure measured using piezoforce microscopy. The black and white regions correspond to opposite orientations of the ferroelectric polarization along the z axis. Note that the domain structure is isotropic, in spite of the layered crystal structure.

tron microscopy to meet at vortex cores²⁴. Importantly (and unusually), while this mode lowers the symmetry to that of a polar space group it carries no net polarization, as any net local polarity vanishes macroscopically due to the non-zero mode wave vector. A secondary mode of Γ_2^- symmetry (referring to the parent space group), which does not further lower the symmetry, provides the ferroelectric polarization (Fig. 1(c)). While the orientation of this secondary ferroelectric polarization is set by the in- or out- tilt of the K_3 mode and does not result in additional domains, it is essential for our experiments as it allows the straightforward imaging of the domain structure using piezoresponse force microscopy (PFM). Indeed PFM measurements reveal that domains of alternating polarization are locked to the trimerization domains around vortex cores^{24,28} yielding appealing six-fold patterns (Fig. 1(d)). Electric-field poling experiments have shown that the vortex cores are protected in the sense that they cannot be annihilated or driven out of the system by an electric field^{24,28}. Surprisingly, the domain structure and density of these topological defects when viewed from the side of the sample is similar to that viewed from the top in spite of the layered crystal structure and uniaxial ferroelectricity²⁸ (Fig. 1(d)). This absence of anisotropy in the domain structure allows for straightforward determination of the defect densities from two-dimensional top-view scans of their areal density, rather than requiring a complex three-dimensional analysis.

First-principles calculations²¹ and Landau Theory analysis²⁹ have shown that for small magnitudes of the trimerizing K_3 mode, the polar mode appears only as a

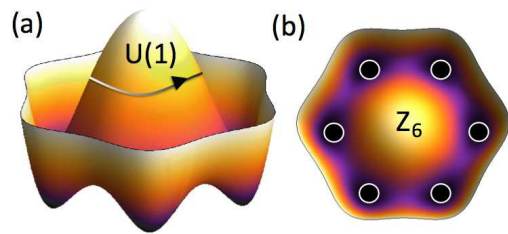


FIG. 2: Mexican-hat potential energy surface of the hexagonal manganites. At high energy (the peak of the hat) the energy is independent of the angle of trimerization, and the system has $U(1)$ symmetry. At lower energy (in the brim of the hat), six of the trimerization angles become favorable (white circles), and the symmetry reduces to the sixfold discrete symmetry described by Z_6 .

third-order term, and so the magnitude of the ferroelectric polarization just below T_C is vanishingly small. This is important for two reasons: First, the formation of the domain structure at T_C is not influenced by the system’s attempts to minimize the depolarizing field from the ferroelectric polarization. Strong evidence for this is given by the large numbers of electrostatically unfavorable head-to-head and tail-to-tail domain walls that form in $RMnO_3$, but rarely occur in conventional ferroelectrics²⁵. Second, first-principles calculations show that the energy lowering provided by the condensation of the K_3 mode is independent of the angle of the tilt until the polar mode subsequently develops⁵⁰²⁹. This means that the potential below the phase transition temperature is given by the continuous “Mexican hat” form (Fig. 2). The discrete nature of the lattice does not manifest until lower temperatures when the domain structure is already determined. As a result we can use the mathematics of continuous symmetries which are usually assumed in the Kibble-Zurek mechanism. In this language, the full rotational symmetry is broken when the polyhedra tilt in the 2π range of angles, resulting in a $U(1)$ vacuum.

For larger magnitudes of the K_3 mode, obtained upon temperature decrease, a cross-over to linear coupling with the polar Γ_2^- mode occurs and the polarization becomes measurably large. This lifts the degeneracy with angle of the K_3 mode and fixes the polyhedra into discrete tilt angles of $0, 2\pi/3$ or $4\pi/3$, described by Z_3 symmetry. The additional degeneracy provided by the direction (“in” or “out”) of the polyhedral tilting gives an additional Z_2 symmetry reduction, resulting in $Z_2 \times Z_3 = Z_6$. It is an open experimental question whether the onset of the Γ_2^- mode, which is observed ~ 300 K below T_C is an “emergence” or an additional isosymmetric phase transition^{21,27}.

II. KIBBLE-ZUREK SCENARIO FOR $RMnO_3$

In this section we first show that the symmetry of $RMnO_3$ results in topologically protected vortex cores as described by the Kibble mechanism. We then analyze the vortex cores using the Zurek scenario to determine the density of topological defects that should be produced as a function of the cooling rate through the phase transition. We use first-principles density-functional theory to evaluate the relevant parameters, and show that our predictions are in excellent agreement with literature data.

A. Kibble mechanism and the formation of topological defects.

The requirements for the formation of topological defects at a phase transition within the Kibble mechanism⁸ are (i) a spontaneous symmetry breaking and (ii) a change in symmetry across the phase transition that corresponds to a non-trivial homotopy group. The trimerization transition in $RMnO_3$ clearly fulfils the first condition; next we show that it also fulfils the second.

As discussed earlier, in the temperature range just below the phase transition, $RMnO_3$ exhibits a continuous symmetry; this allows us to use the methods and results of homotopy theory – which are developed for continuous symmetry groups – to assess the topology of $RMnO_3$. It is established within homotopy theory that the symmetry characteristics of the order parameter, in our case $U(1)$, can be used to assess the topological characteristics of a phase transition. To make the assessment, the order parameter symmetry is first mapped onto an n -dimensional sphere. In the case of the $U(1)$ symmetry, this is a one-dimensional circle, S^1 . Next a function called the homotopy group, π_k , which describes the topological nature of the order parameter symmetry is defined. If π_k differs from the identity, then it is non-trivial and topological defects are formed. It has been known since the 1960's³⁰ that $\pi_k(S^1)$ is indeed non-trivial and in fact produces one-dimensional topological singularities, called strings or vortex cores³¹. Therefore the vortex cores in $RMnO_3$ are mathematically topologically protected, in concordance with their physical topological protection – their resistance to annihilation by an electric field – that we discussed earlier^{24,28}. We note also that within the Kibble mechanism the topological defects are remnants of the parent phase trapped within the lower symmetry phase. For $RMnO_3$ this implies that the high-symmetry paraelectric phase is preserved at the meeting point of the six domains defining a vortex core.

B. Zurek scenario for $RMnO_3$.

Within the Zurek scenario, the density of topological defects formed during a spontaneous symmetry breaking

phase transition described by the Kibble mechanism follows a power-law dependence on the rate at which the transition is crossed^{9,32}. In this section we first relate the material properties of $RMnO_3$ to the parameters in the Zurek scenario. We then evaluate their magnitudes to predict quantitatively the temperature dependence of the defect formation within the Kibble-Zurek mechanism.

Zurek's approach relies on the notion of competing timescales: The first relevant timescale is the time it takes for one region of the system to communicate its choice of vacuum state with another. This time becomes divergently long towards the critical temperature as the correlation length diverges, a phenomenon termed “critical slowing down”. The second is the quench time τ_q that the system spends cooling through the phase transition. The size of the domains is set at the temperature $T_C + \Delta T_f$ where the communication distance across which information can be transferred during the progressing phase transition becomes equal to the correlation length $\xi(T)$ (Fig. 3). While the correlation $\xi(T)$ continues to diverge as the temperature further approaches T_C , the communication length remains unchanged, and the system is unable to adapt to its increase. As consequence a “freeze-out” occurs in the temperature interval between $T_C + \Delta T_f$ and $T_C - \Delta T_f$: The size of the correlated regions is unable to increase and so the domain size is fixed at the value $\xi(T_C + \Delta T_f)$ (Fig. 3). For fast cooling through the transition, the distance over which information can be transferred during the transition is small, and becomes equal to the correlation length at small values of $\xi(T)$. Therefore freeze-out occurs when the domain size is small (and consequently the number of topological defects is large). In contrast, for slow cooling, the distance for information transfer is large, and does not become equal to $\xi(T)$ until close to the phase transition temperature, where $\xi(T)$ is large. In this case large domains, with fewer topological defects, form.

Here we summarize the derivation of the density of topological defects as a function of quench rate through the phase transition within the Kibble-Zurek mechanism. For a detailed derivation we recommend particularly Ref.³³. First, we use critical scaling: As the system approaches T_C , the correlation length, ξ , and relaxation time, τ , diverge as

$$\begin{aligned}\xi(T) &= \xi_0 \left| 1 - \frac{T}{T_C} \right|^{-\nu} \\ \tau(T) &= \tau_0 \left| 1 - \frac{T}{T_C} \right|^{-\mu}\end{aligned}$$

where ξ_0 is the zero-temperature correlation length and τ_0 is the zero-temperature time, which is equal to ξ_0 divided by the speed of information transfer in the system. Both ξ_0 and τ_0 are system-dependent quantities. ν and μ are critical exponents that are determined by the universality class of the phase transition, that is its general behaviour as determined by the symmetry properties of the phase transition, irrespective of the material proper-

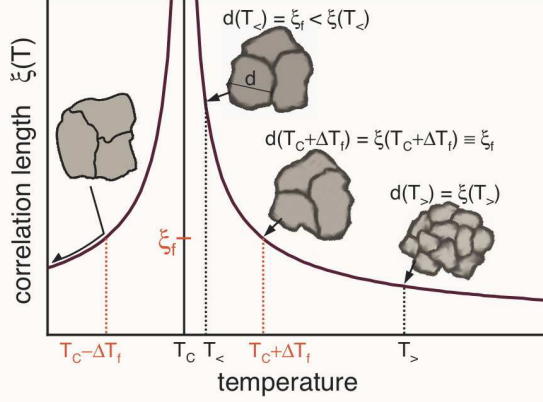


FIG. 3: Domain formation in the Kibble-Zurek scenario. Above T_C fluctuating regions of lateral extension d with uniform orientation of the emerging order parameter occur (fuzzy patches). At high temperature ($T_> > T_C + \Delta T_f$) the size of the correlated regions is determined by the correlation length (purple curve). At temperature $T = T_C + \Delta T_f$ a freeze-out of the lateral extension d begins. Below the freeze-out temperature, Fluctuations continue to occur but the lateral extension of the fluctuating regions can no longer follow the diverging correlation length while the system continues to cool. The size of the fluctuation regions in this range, for example at $T_<$ remains set by the correlation length at the freeze-out temperature, $\xi(T_C + \Delta T_f)$, and corresponds to the “communication length” which is the distance that information can propagate during the time in which the system cools from $T_C + \Delta T_f$ to $T_C - \Delta T_f$. Below $T_C - \Delta T_f$ stable domains of the lateral extension $\xi(T_C + \Delta T_f)$ form (areas confined by black lines).

ties of the specific system.

Assuming that the temperature varies linearly with time near the phase transition, and taking $t = 0$ at $T = T_C$, it is clear that $T = T_C + t \times r_q$, where r_q is the cooling rate. Rearranging this expression yields

$$\left|1 - \frac{T}{T_C}\right| = \frac{r_q t}{T_C} = \frac{t}{\tau_q}$$

where $\tau_q = \frac{T_C}{r_q}$ divided by the cooling rate, is called the “quench time”.

The speed at which information is transferred in the material is then given by the characteristic velocity,

$$c(T) = \frac{\xi(T)}{\tau(T)} = \frac{\xi_0}{\tau_0} \left|1 - \frac{T}{T_C}\right|^{\mu-\nu}$$

and the corresponding distance over which information can propagate in time t is

$$\begin{aligned} \int_0^t c(T(t')) dt' &= \frac{\xi_0}{\tau_0} \int_0^t \left(\frac{t'}{\tau_q}\right)^{\mu-\nu} dt' \\ &= \frac{1}{1 + \mu - \nu} \frac{\xi_0}{\tau_0} \tau_q \left|1 - \frac{T}{T_C}\right|^{1+\mu-\nu} \end{aligned}$$

where in the last step we have substituted $t = \left|1 - \frac{T}{T_C}\right| \tau_q$.

Equating the distance over which information can propagate to the correlation length yields an expression for the freeze-in temperature, T_f :

$$\frac{1}{1 + \mu - \nu} \frac{\xi_0}{\tau_0} \tau_q \left|1 - \frac{T_f}{T_C}\right|^{1+\mu-\nu} = \xi_0 \left|1 - \frac{T_f}{T_C}\right|^{-\nu}$$

so

$$\left|1 - \frac{T_f}{T_C}\right| = \left((1 + \mu - \nu) \frac{\tau_0}{\tau_q}\right)^{\frac{1}{1+\mu}}$$

At temperature T_f , the domain sizes are frozen in with a characteristic length-scale given by the information propagation distance (which is equal to the correlation length) at the freeze-in temperature:

$$\xi_f = \xi_0 (1 + \mu - \nu)^{\frac{\nu}{1+\mu}} \left(\frac{\tau_q}{\tau_0}\right)^{\frac{\nu}{1+\mu}}$$

Formally, this corresponds to the length-scale of the vortex “strings”, that is the three-dimensional continuation of the vortex cores through the bulk of the sample. The number of vortex intersections per unit area, n , is then approximately equal to the length of vortices per unit volume, $\frac{1}{\xi_f^3}$, giving

$$n \approx \frac{1}{\xi_0^3} \left(\frac{\tau_0}{\tau_q}\right)^{\frac{3\nu}{1+\mu}}$$

To apply the linear Zurek scaling law given in Eq. (II B) to the hexagonal manganites we next identify the relevant time- and length-scales in the system, and evaluate their magnitudes. Our electronic structure calculations were performed using density functional theory within the local density plus Hubbard- U approximation following the Liechtenstein approach³⁴ with the double-counting corrections treated in the fully localized limit. Following previous literature studies²¹, we set the LDA+ U parameters on the Mn $3d$ orbitals to $U = 8$ and $J = 0.88$ eV respectively and enforced an A-type antiferromagnetic ordering. We used the projector-augmented wave method for core-valence partitioning³⁵, which significantly reduces the required plane-wave energy cutoff, and carefully tested the convergence of plane-wave cutoff and k-point sampling.

The zero-temperature correlation length, ξ_0 , is usually equated with the zero-temperature domain wall width in ferroelectrics. In order to extract this value we performed density functional calculations within the LDA+ U method using the VASP code^{36,37}. We constructed supercells containing two 180° domain walls and in turn 120, 180, 240 and 300 atoms. We fixed the lattice constants of the supercells to those of the relaxed single-domain unit cell, and then optimized the internal positions until the forces acting on all atoms converged to less

than 0.01 eV/Å respectively. We initialized a different trimerization phase and ferroelectric orientation within adjacent domains, and subsequently performed full relaxations on the structures; in all cases the system remained in the metastable multi-domain state. For all supercell sizes, we found that the structural phase defined by either the tilt of the MnO bipyramids or the direction of off-centring of the Y ions changes abruptly at the domain walls, indicating an effective domain wall width close to zero. This is consistent with a recent experimental electron microscopy study³⁸, and sets an upper limit on ξ_0 of ~ 1 Å.

To calculate the characteristic timescale of the system, $\tau_0 = \frac{\xi_0}{s}$, we require s , which is the speed at which the system communicates the lattice distortion as it passes through the phase transition. For solid-state systems, s is given by the speed of sound. To calculate the speed of sound at zero kelvin we used the ABINIT⁵¹ software package^{39,40} to optimize the structure of a 10-atom unit cell, then calculated the full phonon band structure using frozen-phonon techniques. A supercell was constructed with doubling and trebling in each of the directions required to sample the first Brillouin zone, then symmetry-distinct displacements were made to construct the full matrix of interatomic force constants. The dynamical matrix was diagonalized along each of the high symmetry lines shown in the phonon band structure using Fourier interpolation.^{41,42} The speed of sound was then extracted from the calculated phonon band structure by fitting the acoustic branch with a polynomial, then evaluating the group velocity

$$v_g = \left. \frac{\partial \omega}{\partial k} \right|_{\vec{k}=0}$$

. The relevant velocity for our Kibble-Zurek fit is the doubly degenerate branch with the atoms displacing in plane and the wavevector propagating in plane. For this branch we obtained $v_g = 640 \text{ m.s}^{-1}$.

Finally, for comparison with quenching experiments we also need the Curie temperature, T_C , which relates τ_q to the cooling rate, r_q through $r_q = \frac{T_C}{\tau_q}$. This is known experimentally to be ~ 1400 K, with the exact number depending on the R ion.

Next we extract the critical exponents by identifying that, as in the case of the superfluid transition in ^4He , the $RMnO_3$ transition belongs to the universality class denoted as the 3D XY model. The values of the critical exponents for this universality class have been calculated using Monte Carlo simulations⁴³ to be $\nu = 0.6717$ and $\mu = 1.3132$, giving a Kibble-Zurek scaling exponent of $\frac{2\nu}{1+\mu} \approx 0.29$. Taking the values introduced so far, with our upper limit for ξ_0 , we find that domains of $5\mu\text{m}$ width should be formed for a quench time of $\tau_q \sim 40$ min (corresponding to a cooling rate of ~ 0.5 K/s), and domains of $40 \mu\text{m}$ in around one month (cooling rate ~ 1.5 K/hour). These are readily experimentally accessible cooling rates.

In Fig. 5(d) we compare our predicted scaling behavior with recently reported vortex densities measured as

a function of cooling rate in $ErMnO_3$ (red circles)¹. The agreement in scaling behavior between the experiment and the Kibble-Zurek prediction is excellent. Note in particular that the scaling exponent matches exactly the theoretical prediction; this is the first time to our knowledge that such good agreement has been obtained. We obtain the best match with a value of zero-temperature correlation length of 0.06 Å (solid red line), consistent with the approximately zero domain wall width obtained in our density functional calculations. Hence, $RMnO_3$ is the first system to show model Kibble-Zurek behavior in the laboratory.

We thus find a unique situation in $RMnO_3$. Topologically, it is a model system for the experimental verification of the Kibble-Zurek mechanism. In the temperature range where the Kibble-Zurek mechanism is expected to govern the formation of domains and the distribution of vortex-core singularities, the unwanted ferroelectric polarization which could influence domain formation is effectively absent. However, at room temperature the coupling of the distortive order parameter to the now finite ferroelectric polarization allows straightforward imaging of the topology and vortices via spatially resolved measurements of the ferroelectric domain structure. And finally, a distinguishable range of domain sizes and hence defect densities is obtained for an experimentally accessible range of cooling rates through the primary distortive phase transition at T_C .

III. BEYOND THE KIBBLE-ZUREK LIMIT

The Kibble-Zurek mechanism applies only to the regime in which the system has time to respond adiabatically to the cooling until the freeze-out temperature, $T_C + \Delta T_f$ is reached. For faster quenching, it is expected that the Kibble-Zurek mechanism should break down and be replaced by a dynamics that is largely unknown. The unique combination of properties in $RMnO_3$ allows us to continue to increase the cooling rate beyond those explored in Ref.¹ to investigate the evolution out of the Kibble-Zurek regime; we explore this range next.

For our experiment we chose $YMnO_3$ rather than the $ErMnO_3$ that was used in Ref.¹ because of the greater thickness of our $YMnO_3$ samples. The experimental procedure applied to the flux-grown, c -oriented single crystal $YMnO_3$ platelets is shown in Fig. 4. For our annealing experiments we used a conventional chamber furnace (carbolite CWF 13/13) which allows for temperatures from room temperature up to 1550 K exceeding considerably the $T_C \approx 1270$ K of our $YMnO_3$ samples. First we performed a pre-annealing at 1420 K for 24 h under constant oxygen flow of 0.2 l/min. In the second step the samples were annealed again with a different cooling rate. Up to 8 K/min the temperature gradient was controlled by the furnace, higher rates were obtained by removing the fused-silica cell with the sample from the furnace and measured by an infrared camera (InfraTec

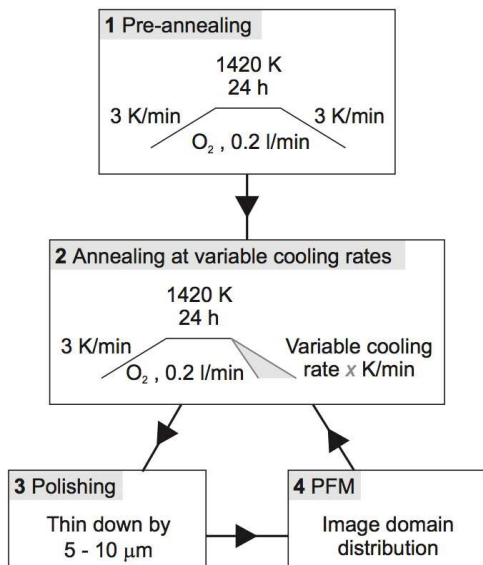


FIG. 4: Sketch of the annealing procedure. After pre-annealing the samples are heated to 1420 K with a hold time of 24 h and subsequent cooling at rates between 0.1 and 1360 K/min. After the annealing cycle they are thinned down 5-10 μm by polishing in order to access the domain structure formed in the true three-dimensional bulk of the sample.

VarioCAM). The annealing was followed by thinning the samples down by 5-10 μm using Al_2O_3 and polishing chemically-mechanically with 32 nm grain-size slurry. In the last step the ferroelectric domain structure was imaged using piezoresonance force microscopy^{1,28}. We used a commercial scanning force microscope (Solaris, NT-MDT) operated in contact mode and applied an AC-voltage of 14 V_{pp} at a frequency of ~ 40 kHz to a conductive Pt-Ir coated probe (NSC 35, Mikromasch). The out-of-plane component of the piezoelectric response was recorded by the in-phase output channel of an external lock-in amplifier (SR830, Stanford Research) with a typical sensitivity of 200 μV and time constant of 10 ms. Finally, the area density of vortices was extracted from the PFM images.

In Fig. 5 (a-c) we show the measured distribution of domains in YMnO_3 for fast cooling rates of 3, 195, and 1360 K/min, and in Fig. 5(d) we plot our measured vortex core densities as a function of cooling rate (blue circles). The independence of the vortex core density to the choice of R is confirmed by the smooth connection between the ErMnO_3 (red circles) and YMnO_3 (blue circles) data points in Fig. 5. Following a crossover occurring between 0.3 and 3 K/min (see Fig. 5(d)) we observe a striking “anti-Kibble-Zurek” behavior in the measured density of domain vortex cores as a function of cooling rate: Within the fast-cooling regime, an increase in the cooling rate leads to a *lowering* of the density of vortex cores (larger domains); this behaviour is opposite to that predicted by the standard Kibble-Zurek mechanism. We emphasize that the behaviour is highly repro-

ducible: We repeated our measurements on YMnO_3 samples grown in different batches, and verified that there are no drift effects in consecutive annealing cycles. We therefore conclude that our results indicate an evolution out of the Kibble-Zurek regime at a cooling rate of ~ 1 K/min in the hexagonal manganites. This crossover point corresponds to a correlation length (and hence a crossover domain size) of $\sim 2.2 \mu\text{m}$, and a relaxation time of $\sim 4.1 \times 10^{-4}$ s, with a characteristic information transfer velocity of $\sim 5.4 \times 10^{-3}$ m/s, considerably reduced from the speed of sound by the critical slowing down.

IV. DISCUSSION: POSSIBLE ORIGINS OF THE KIBBLE-ZUREK / “ANTI-KIBBLE-ZUREK” CROSSOVER

A number of possible deviations from Kibble-Zurek behavior have been discussed in the literature, but none of them are consistent with our measurements. Zurek² showed that vortex–anti-vortex annihilation becomes significant at fast quench rates where domains are smaller and topological defects are closer together. Such vortex–anti-vortex annihilation causes a leveling off of the rate at which the density of vortex cores increases with cooling rate, but not the decrease in density that we observe. The effect of nonlinearity in the quench rate on the density of defects has been calculated to yield a modified scaling law⁴⁴, which again would not cause our observed turnaround at fast cooling rates. In Ref.¹ it was suggested that the observed production of defect–anti-defect pairs could be the result of a Kosterlitz-Thouless transition⁴⁵, in which vortex–anti-vortex pairs are formed above the transition temperature and annihilate as the system is cooled. As a result, more vortex cores survive during a fast quench when the pairs do not have time to annihilate. This is the opposite of our observed fast-quenching behavior. In addition, a Kosterlitz-Thouless system would show a dramatic change in the density of vortices after repeated annealing cycles as well as a dependence on the temperature at which the quench begins, neither of which we observe.

A possible extrinsic influence on the domain structure could be differences in chemical defect concentration caused by the different cooling rates, such as off-stoichiometry, anti-site formation, or charge screening at the domain-walls. To test for this possibility, we heated our samples to within 2% of the transition temperature, and annealed them at this temperature for six hours under the conditions described above. No changes in the domain structure were observed on heating until 1270 K (just below T_C), at which point minor isolated domain wall movements, and, once, the formation of a vortex–anti-vortex pair were observed. On heating to 1320 K (just above T_C), a completely new, but statistically identical domain pattern was obtained. These data and the aforementioned reproducibility of our data points in Fig.

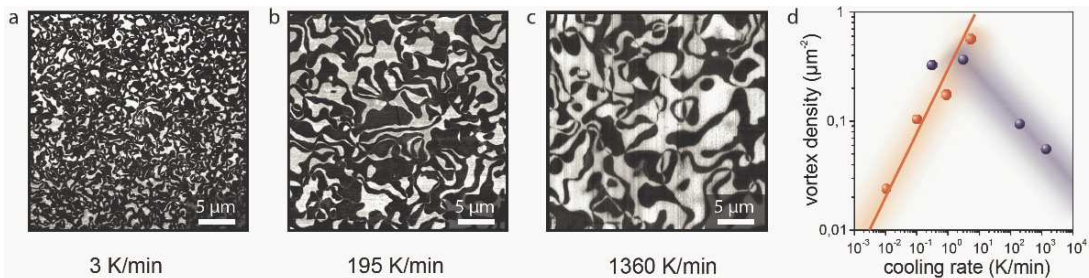


FIG. 5: (a) to (c) Distribution of ferroelectric domains in z -oriented YMnO_3 samples after annealing cycles at different cooling rates. The images are obtained using PFM on an area of $30 \times 30 \mu\text{m}^2$ and reveal a striking ‘anti-Kibble-Zurek’ behavior with higher cooling rates leading to larger domains. (d) Areal vortex core density as a function of cooling rate for slow cooling (red circles, Ref.¹) and fast cooling (blue circles, this work). Note the turnover in the cooling-rate dependence of the vortex-core density occurring between rates of 0.3 and 3 K/min. The red solid line is the result of our *ab initio* application of the Kibble-Zurek scenario with parameters from first-principles calculations.

5 show that chemical drift effects do not play a role.

We conclude therefore, that the most likely origin of the transition out of the Kibble-Zurek regime in RMnO_3 is the breakdown of the assumption that the system is able to respond adiabatically to the cooling at high temperatures, above the freeze-out temperature $T_C + \Delta T_f$. Our observed behavior in the fast-cooling regime – slower cooling leading to a larger number of smaller domains – is of course reminiscent of nucleation-dominated behavior, with an activation energy for formation of the low symmetry phase from the high symmetry phase. Nucleation-dominated phase transitions show characteristic first-order behavior, and a longer time spent at the transition allows a larger number of smaller domains to nucleate. We note that at the freeze-out temperature corresponding to the crossover quench-rate, the order parameter for the trimerization, $\eta = \left(\frac{T-T_C}{T_C}\right)^\beta$, has already reached 0.5% of its saturation value, taking the experimental value of $\beta = 0.29$ ⁴⁶. It is possible that this provides a sufficient discontinuity from the zero value to induce a first-order response. An alternative scenario is the fluctuation-induced first-order behaviour proposed for prototypical second-order phase transitions such as the normal-to-superconducting transition and for the nematic-smectic transition in liquid crystals⁴⁷, both of which belong to the same universality class – the 3D XY model – as the hexagonal manganites. Such an induced-first-order transition could also explain the current controversy regarding the order of the trimerization transition in the hexagonal manganites, with most experiments showing second-order behavior, but occasional reports of first-order characteristics.

V. SUMMARY

In Summary, we have shown that the multiferroic hexagonal manganites, RMnO_3 , are model systems for

testing the Kibble-Zurek scenario. Mathematically, they fulfil the symmetry requirements for the formation of topological defects, and practically, the defects are readily detectable, the quench rate can be varied over a wide range of relevant timescales, and extrinsic factors that might influence the phase transition behavior are absent. Our quantitative calculations of topological defect density as a function of cooling rate using the conventional Kibble-Zurek model and parameters obtained using density functional theory, yield excellent agreement with literature data in the slow cooling limit where the conventional Kibble-Zurek mechanism is applicable. Our measurements of defect density at fast cooling rates, however, reveal a surprising, apparently ‘anti-Kibble-Zurek’ behavior in which faster cooling yields lower defect densities, reminiscent of a nucleation-dominated phase transition. Since the expansion of the universe during the inflationary period was rapid^{48,49}, the turn-around in vortex density which we find here at fast-cooling rates may be applicable, and the observed deficiency of cosmic strings in the cosmic microwave background³ could be rationalised by the decrease in defect density observed in the anti-Kibble-Zurek regime.

Acknowledgments

We thank Pierre Tolédano, Maxim Mostovoy and Ali Mozaffari for invaluable discussions, Sang-Wook Cheong for sharing the data in Figure 5(d) prior to its publication, and the Cosmic Superstrings Meeting (Portsmouth, UK, 2011) for allowing us to attend and discuss our ideas. This work was supported financially by the ETH Zürich. MF thanks the IMI Program of the National Science Foundation under Award No. DMR-0843934, managed by the International Center for Materials Research, UC Santa Barbara, for sabbatical support.

-
- ¹ S. C. Chae, N. Lee, Y. Horibe, M. Tanimura, S. Mori, B. Gao, S. Carr, and S.-W. Cheong, Phys. Rev. Lett., in press (2012), arXiv:1203.5371v1.
- ² A. Yates and W. H. Zurek, Phys. Rev. Lett. **80**, 5477 (1998).
- ³ M. Hindmarsh, C. Ringeval, and T. Suyama, Phys. Rev. D **D81**, 063505 (2010).
- ⁴ A. Vilenkin and E. P. S. Shellard, *Cosmic Strings and Other Topological Defects* (Cambridge University Press, 1994).
- ⁵ T. Vachaspati, Phys. Rev. D **80**, 063502 (2009).
- ⁶ N. Bevis, M. Hindmarsh, M. Kunz, and J. Urrestilla, Phys. Rev. Lett. **100**, 021301 (2008).
- ⁷ R. Jeannerot, J. Rocher, and M. Sakellariadou, Phys. Rev. D **68**, 103514 (2003).
- ⁸ T. W. B. Kibble, J. Phys. **A9**, 1387 (1976).
- ⁹ W. H. Zurek, Nature **317**, 505 (1985).
- ¹⁰ P. C. Hendry, N. S. Lawson, R. A. M. Lee, P. V. E. McClintock, and C. D. H. Williams, Nature **368**, 315 (1994).
- ¹¹ M. E. Dodd, P. C. Hendry, N. S. Lawson, P. V. E. McClintock, and C. D. H. Williams, Phys. Rev. Lett. **81**, 3703 (1998).
- ¹² R. J. Rivers, Phys. Rev. Lett. **84**, 1248 (2000).
- ¹³ C. Bauerle, Y. M. Bunkov, S. N. Fisher, H. Godfrin, and G. R. Pickett, Nature **382**, 332 (1996).
- ¹⁴ V. M. H. Ruutu, V. B. Eltsov, A. J. Gill, T. W. B. Kibble, M. Krusius, B. V. G. E. Makhlin, Yu. G. Annd Placais, and W. Xu, Nature **382**, 334 (1996).
- ¹⁵ R. Monaco, J. Mygind, R. J. Rivers, and V. P. Koshelets, Phys. Rev. B **80**, 180501 (2009).
- ¹⁶ R. Carmi and E. Polturak, Phys. Rev. B **60**, 7595 (1999).
- ¹⁷ C. N. Weiler, T. W. Neely, D. R. Scherer, S. Bradley, Ashton, J. Davis, Matthew, and B. P. Anderson, Nature **455**, 948 (2008).
- ¹⁸ S. Ducci, P. L. Ramazza, W. Gonzalez-Vinas, and F. T. Arecchi, Phys. Rev. Lett. **83**, 5210 (1999).
- ¹⁹ I. Chuang, R. Durrer, N. Turok, and B. Yurke, Science **251**, 1336 (1991).
- ²⁰ B. B. van Aken, T. T. M. Palstra, A. Filippetti, and N. A. Spaldin, Nature Mater. **3**, 164 (2004).
- ²¹ C. J. Fennie and K. M. Rabe, Phys. Rev. B **72**, 100103(R) (2005).
- ²² M. Fiebig, T. Lottermoser, D. Fröhlich, A. V. Goltsev, and R. V. Pisarev, Nature **419**, 818 (2002).
- ²³ T. Lottermoser, T. Lonkai, U. Amann, D. Hohlwein, J. Ihringer, and M. Fiebig, Nature **430**, 541 (2004).
- ²⁴ T. Choi, Y. Horibe, H. T. Yi, Y. J. Choi, W. Wu, and S.-W. Cheong, Nat. Mater. **9**, 253 (2010).
- ²⁵ D. Meier, J. Seidel, A. Cano, K. Delaney, Y. Kumagai, M. Mostovoy, N. A. Spaldin, R. Ramesh, and M. Fiebig, Nat. Mater. **11**, 284 (2012).
- ²⁶ H. L. Yakel, W. C. Koehler, E. F. Bertaut, and E. F. Forrat, Acta Cryst. **16**, 957 (1963).
- ²⁷ T. Lonkai, D. G. Tomuta, U. Amann, J. Ihringer, R. W. A. Hendrikx, D. M. Tobben, and J. A. Mydosh, Phys. Rev. B **69**, 134108 (2004).
- ²⁸ T. Jungk, Á. Hoffmann, M. Fiebig, and E. Soergel, Appl. Phys. Lett. **97**, 012904 (2010).
- ²⁹ S. Artyukhin, K. T. Delaney, N. A. Spaldin, and M. Mostovoy, In preparation (2012).
- ³⁰ M. A. Kervaire and J. W. Milnor, Ann. of Math., Second Series **77**, 504 (1963).
- ³¹ T. W. B. Kibble, *Classification of topological defects and their relevance to cosmology and elsewhere, in Topological Defects and the Non-Equilibrium Dynamics of Symmetry Breaking Phase Transitions*, vol. C 549 of *NATO Science Series* (Kluwer Academic Publishers, 2000).
- ³² M. Hindmarsh and A. Rajantie, Phys. Rev. Lett. **85**, 4660 (2000).
- ³³ T. W. B. Kibble, in *Patterns of Symmetry Breaking* (2003), vol. 127 of *NATO Science Series II: Mathematics, Physics and Chemistry*, pp. 3–36, proceedings of the Conference of the NATO-Advanced-Study-Institute on Patterns of Symmetry Breaking, Cracow, Poland, September 2002.
- ³⁴ A. I. Liechtenstein, V. I. Anisimov, and J. Zaanen, Phys. Rev. B **52**, R5467 (1995).
- ³⁵ P. E. Blöchl, Phys. Rev. B **50**, 17953 (1994).
- ³⁶ G. Kresse and J. Hafner, Phys. Rev. B **47**, 558 (1993).
- ³⁷ G. Kresse and J. Furthmüller, Phys. Rev. B **54**, 11169 (1996).
- ³⁸ Q. H. Zhang, L. J. Wang, X. K. Wei, R. C. Yu, L. Gu, A. Hirata, M. W. Chen, C. Q. Jin, Y. Yao, Y. G. Wang, et al., Phys. Rev. B **85**, 020102 (R) (2012).
- ³⁹ X. Gonze, J.-M. Beuken, R. Caracas, F. Detraux, M. Fuchs, G.-M. Rignanese, L. Sindic, M. Verstraete, G. Zerah, F. Jollet, et al., Comp. Mater. Sci. **25**, 478 (2002).
- ⁴⁰ X. Gonze, B. Amadon, P.-M. Anglade, J.-M. Beuken, F. Bottin, P. Boulanger, F. Bruneval, D. Caliste, R. Caracas, M. Cote, et al., Comp. Phys. Commun. **180**, 2582 (2009).
- ⁴¹ A. Togo, F. Oba, and I. Tanaka, Phys. Rev. B **78**, 134106 (2008).
- ⁴² K. Parlinski, Z. Q. Li, and Y. Kawazoe, Phys. Rev. Lett. **78**, 4063 (1997).
- ⁴³ M. Camprostrini, M. Hasenbusch, A. Pelissetto, and E. Vicari, Phys. Rev. B **74**, 144506 (2006).
- ⁴⁴ S. Mondal, K. Sengupta, and D. Sen, Phys. Rev. B **79**, 045128 (2009).
- ⁴⁵ J. M. Kosterlitz and D. J. Thouless, Journal of Physics C Solid State Physics **6**, 1181 (1973).
- ⁴⁶ A. S. Gibbs, K. S. Knight, and P. Lightfoot, Phys. Rev. B **83**, 094111 (2011).
- ⁴⁷ B. I. Halperin, T. C. Lubensky, and S.-K. Ma, Phys. Rev. Lett. **32**, 292 (1974).
- ⁴⁸ A. H. Guth, Phys. Rev. D **23**, 347 (1981).
- ⁴⁹ A. A. Starobinsky, Physics Letters B **117**, 175 (1982).
- ⁵⁰ Note that the Landau free energy derived in Ref.²⁹ has a branch cut in the trimerization angle that gives a signature of topological protection if the angle rotates through the branch cut when traced round the vortex core.
- ⁵¹ The ABINIT code is a common project of the Université Catholique de Louvain, Corning Incorporated, and other contributors (URL <http://www.abinit.org>).